

Article

SnO₂/Diatomite Composite Prepared by Solvothermal Reaction for Low-Cost Photocatalysts

Haiyan Jiang ¹, Rui Wang ², Daohan Wang ¹, Xiaodong Hong ^{2,*} and Shaobin Yang ²

¹ College of Environmental Science and Engineering, Liaoning Technical University, Fuxin 123000, China; yunwen2004@126.com (H.J.); hxdhit@163.com (D.W.)

² College of Materials Science and Engineering, Liaoning Technical University, Fuxin 123000, China; a18341843530@163.com (R.W.); lgdysb@163.com (S.Y.)

* Correspondence: hongxiaodong@lntu.edu.cn; Tel.: +86-138-4187-7730

Received: 29 November 2019; Accepted: 10 December 2019; Published: 13 December 2019



Abstract: Abundant contaminants in wastewater have a negative effect on the natural environment and ecology. Developing highly efficient photocatalysts is a practical strategy to solve the pollution issue. In order to prevent the agglomeration of SnO₂ nanoparticles and improve the photocatalytic efficiency, porous diatomite is adopted as a low-cost template to load monodispersed SnO₂ nanoparticles by solvothermal reaction and sintering method. Through adjusting the mass of reactants, monodispersed SnO₂ nanoparticles (~15 nm) generated on diatomite template achieved the maximum specific surface area of 23.53 m²·g⁻¹. When served as a photocatalyst for degrading rhodamine B (Rh B) and methylene blue (MB), the composite presents an excellent photocatalytic activity close to pure SnO₂, and achieves the fast degradation of Rh B and MB dye in 60 min. The degradation process is in well agreement with the first-order kinetic equation. The superior photocatalytic performance of SnO₂/diatomite composite is attributed to the physical adsorption of dye molecules on the pores of diatomite, and the superior photocatalytic activity of monodispersed SnO₂ nanoparticles. Due to the low-cost of diatomite and the easy preparation of SnO₂ nanoparticles, the SnO₂/diatomite composite has a promising application prospect, even better than pure SnO₂ photocatalyst.

Keywords: SnO₂; diatomite; degradation; photodegradation; organic dyes

1. Introduction

A great amount of industrial wastewater seriously pollutes rivers and water sources, which brings great harm to animals, plants and human. Therefore, the controllable degradation of organic pollutants in wastewater is crucial to alleviate the damage to natural environment and ecology. Aiming at degrading the poisonous organic pollutants in wastewater, photocatalytic technology has been attracted much attention in recent years. The metal oxides semiconductors can be acted as high performance photocatalysts [1,2]. Under the irradiation of visible light, semiconductor materials can be excited to degrade organic pollutants into CO₂, H₂O and inorganic ions, and purify the wastewater. Among various semiconductor photocatalysts, SnO₂ is an important wide band gap, n-type semiconductor material [3,4], which has abundant surface lattice oxygen defects. Moreover, SnO₂ is a kind of surface resistance-controlled material with a strong adsorption capacity, high specific surface, internal activity, and fast reaction with pollutants, hence the SnO₂ nanoparticles exhibit a superior photocatalytic performance [5]. In order to further improve the photocatalytic efficiency, various SnO₂ nanostructures including nanoparticles, nanowires, spheres and nanorods, have been synthesized by adjusting the surfactants, reactants, reaction temperature and time [6,7]. However, as a photocatalyst, SnO₂ aggregates seriously deteriorate the photocatalytic activity and photocatalytic efficiency. While it is hard to prevent the agglomeration of SnO₂ nanoparticles during a synthesis process.

Therefore, during the synthesis process, the selection of suitable templates is very crucial to control the uniform distribution of SnO₂ nanoparticles. As we all know, SnO₂ is often synthesized on graphene nanosheets to enhance the photocatalytic efficiency [8]. For example, Chen et al. [9] synthesized dense SnO₂ layers on two sides of graphene sheets as high-efficient photocatalysts. Wei et al. [10] synthesized dandelion-like SnO₂ on graphene sheets and presented an excellent photocatalytic performance when degrading Rhodamine B. However, the high cost of graphene or graphene oxide confines the wide application of graphene-metal oxides hybrid photocatalysts. As a cheap porous clay mineral, diatomite derives from a kind of single celled aquatic algae. It has some advantages, such as a low cost, large specific surface area, high porosity and chemical resistance. In the reported works about diatomite-based photocatalysts, diatomite is often acted as porous template to load TiO₂ nanoparticles by sol-gel method [11] or hydrolysis-deposition method [12]. However, up to now, there are only two works about SnO₂/diatomite composites. Zhong et al. [13] synthesized SnO₂ nanowires on diatomite porous substrate. The composite was acted as gas sensing materials for detecting the response to SO₂ gas. Zhen et al. [14] synthesized SnO₂ on diatomaceous earth by hydrothermal method and investigated the potential application in the humidity sensing field. There are no reports about SnO₂/diatomite photocatalysts.

About the synthesis of SnO₂, hydrothermal or solvothermal method is often adopted to synthesize various SnO₂ nanostructures. In our previous work, SnO₂ nanosheets consisted of hierarchical SnO₂ nanoparticles were synthesized on carbonized cotton cloth by solvothermal reaction and sintering method [15]. Considering the easy preparation of monodispersed SnO₂ nanoparticles, the low cost of diatomite, and no reports about SnO₂/diatomite photocatalysts, therefore, we synthesize monodispersed SnO₂ nanoparticles on porous diatomite template by solvothermal reaction and sintering method. Firstly, SnS₂ was synthesized on porous diatomite template by the solvothermal reaction of SnCl₄·5H₂O and thioacetamide in isopropanol. Then, the SnS₂/diatomite composite was sintered at 500 °C in air to produce SnO₂/diatomite composite. Through changing the mass of precursors, four samples were prepared under the different mass ratios of SnO₂ and diatomite as provided in Table 1. The samples were characterized by X-ray diffraction (XRD), scanning electron microscopy (SEM), transmission electron microscopy (TEM) and specific surface analysis (BET). In the photodegradation test, rhodamine B (Rh B) and methylene blue (MB) were adopted as simulated pollutants, and the relationship between SnO₂ contents in composite and photocatalytic activity were discussed in detail. At last, the corresponding photodegradation mechanism of SnO₂/diatomite composite was put forward.

Table 1. The specific surface area of different SnO₂/diatomite composites derived from BET method.

Sample	Diatomite	SD1	SD2	SD3	SD4
SnCl ₄ ·5H ₂ O/thioacetamide	0/0	106/64 mg	212/128 mg	338/192 mg	424/256 mg
SnO ₂ fraction	0	4.9%	7.6%	11.7%	16.5%
Specific surface area/(m ² ·g ⁻¹)	13.72	17.15	23.53	14.95	11.56

2. Results and Discussion

2.1. Composition and Structure of Materials

The XRD patterns of the pure SnO₂, modified diatomite, and SnO₂/diatomite composites are shown in Figure 1. The specific information of SnO₂/diatomite composites is given in Section 3 and Table 1. From the spectrum of diatomite, it can be seen that there are obvious diffraction peaks at 21.98°, 28.44°, 31.46°, 36.08°, 42.66°, 44.84°, 47.06°, 48.61°, 57.08°, and 65.10°. These peaks are just corresponding to (101), (111), (102), (200), (211), (202), (113), (212), (301) and (312) crystal face of SiO₂ [16], which reflect that the diatomite is a kind of porous SiO₂. The characteristic peaks at 26.61°, 33.89°, 37.95°, 51.78°, 54.76°, 54.76°, 61.87°, 64.72°, 65.94°, 71.28° and 78.71° are assigned to the (110), (101), (200), (211), (220), (002), (310), (112), (301), (202), and (321) crystal face of pure SnO₂,

respectively [17]. From the spectra of different SnO₂ loadings on diatomite, the peak intensity of SnO₂ in SD4 sample is obviously higher than other samples, which may be attributed to the highest SnO₂ fraction in the composite (Table 1). In addition, the composites also exhibit the feature peaks of diatomite at 21.98°, 28.44°, 31.46° and 36.08°, which further confirm that SnO₂ particles are generated on the diatomite template successfully.

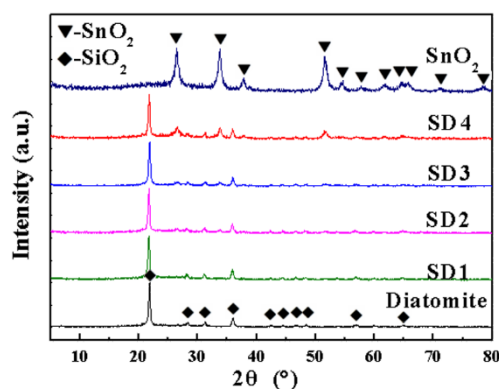


Figure 1. XRD spectra of pure SnO₂, modified diatomite and SnO₂/diatomite composites.

The microstructure of different materials are shown in Figure 2. In the absence of porous template, pure SnO₂ (Figure 2a) exhibits a two-dimensional lamellar structure assembled by nanoparticles, with an average particle size of about 20 nm [18]. The possible reason for the formation of SnO₂ aggregates is no template in the synthesis, resulting in a large number of nano-sized SnO₂ particles assembled and connected together to form a lamellar structure. This aggregation phenomenon can be overcome by adding porous diatomite template during the synthesis process. Figure 2b shows the microstructure of modified diatomite. After the acidification treatment, the surface of the diatomite is smooth, in the form of a disc-shaped porous screen structure with a disc diameter of 20~40 μm and a pore diameter of 100~200 nm. Abundant porous structure ensures the diatomite with a large specific surface area, which can be served as an excellent template to prevent the aggregation of SnO₂ nanoparticles. The microstructure of four SnO₂/diatomite composites are presented in Figure 2c–f. It can be observed that the number of SnO₂ nanoparticles on the surface of diatomite increase gradually with an increase of SnCl₄·5H₂O precursors. When the resultant SnO₂ content is less than 10%, corresponding to SD1 and SD2. There are ultrafine SnO₂ nanoparticles dispersed on the surface of diatomite uniformly (Figure 2c), and the particle diameter of SnO₂ is about 15 nm. At the same magnification of SEM, the SnO₂ particles in the SD2 samples (Figure 2d) were denser than the SD1 sample. When the loading amount of SnO₂ is more than 10%, the SnO₂ nanoparticles are agglomerated on the surface of diatomite, especially for the SD4 sample in Figure 2f, the size of SnO₂ agglomeration is more than 1 μm. The big aggregates undoubtedly reduce the specific surface area and deteriorate the photocatalytic activity of composite. The formation reason of big aggregates can be attributed to the self-aggregate of SnO₂ nanoparticles in a high concentration of SnCl₄·5H₂O precursor. Therefore, under the appropriate precursor concentration, porous diatomite template can effectively suppress the agglomeration of SnO₂ nanoparticles. When the mass of SnCl₄·5H₂O and thioacetamide (TAA) are 212 and 128 mg separately, the resultant SnO₂ content in composite is 7.6%, which achieves the monodispersed distribution of SnO₂ nanoparticles (about 15 nm) on the surface of porous diatomite, and the particle size is even smaller than that of pure SnO₂ (~20 nm) with no diatomite.

In addition, we also observed the microstructure of pure SnO₂ and SnO₂/diatomite-SD2 sample by TEM. Pure SnO₂ is shown in Figure 3a. The SnO₂ aggregates are composed of numerous SnO₂ nanoparticles, and the particle diameter is less than 20 nm. However, from the SnO₂/diatomite composite (SD2) in Figure 3b, there are much more SnO₂ particles covering on the diatomite surface, and the magnified region in Figure 3c just shows the crystalline SnO₂ nanoparticles dispersed on the matrix of amorphous diatomite. The lattice spacing of SnO₂ is 0.334 nm, which is assigned to the

(110) plane of tetragonal SnO_2 . Moreover, the particle size of SnO_2 is less than 15 nm, which is in well agreement with the results obtained by SEM. In addition, the XPS general spectrum of pure SnO_2 was obtained in Figure 3d, the wide survey scan exhibits the feature peaks of Sn and O elements. The high-resolution Sn spectrum was provided in Figure 3e, there are two strong peaks at 495.8 eV and 487.2 eV, corresponding to the spin orbits of $\text{Sn } 3d_{3/2}$ and $\text{Sn } 3d_{5/2}$ respectively. The binding energy gap is 8.6 eV, which is in accordance with the oxidation state of Sn^{4+} . The result further confirmed the formation of SnO_2 , as reflected in the XRD result.

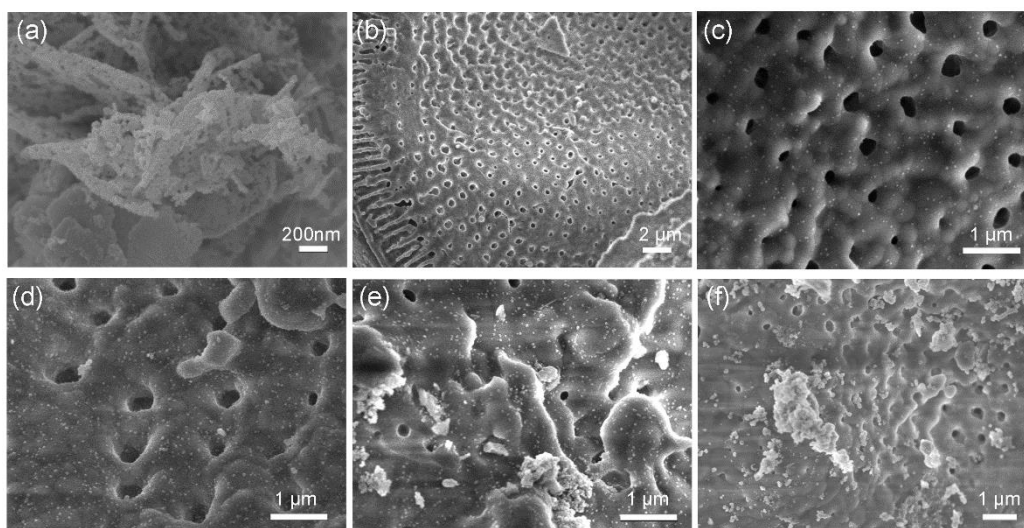


Figure 2. The microstructure of (a) pure SnO_2 , (b) modified diatomite, (c) SD1, (d) SD2, (e) SD3 and (f) SD4 by SEM.

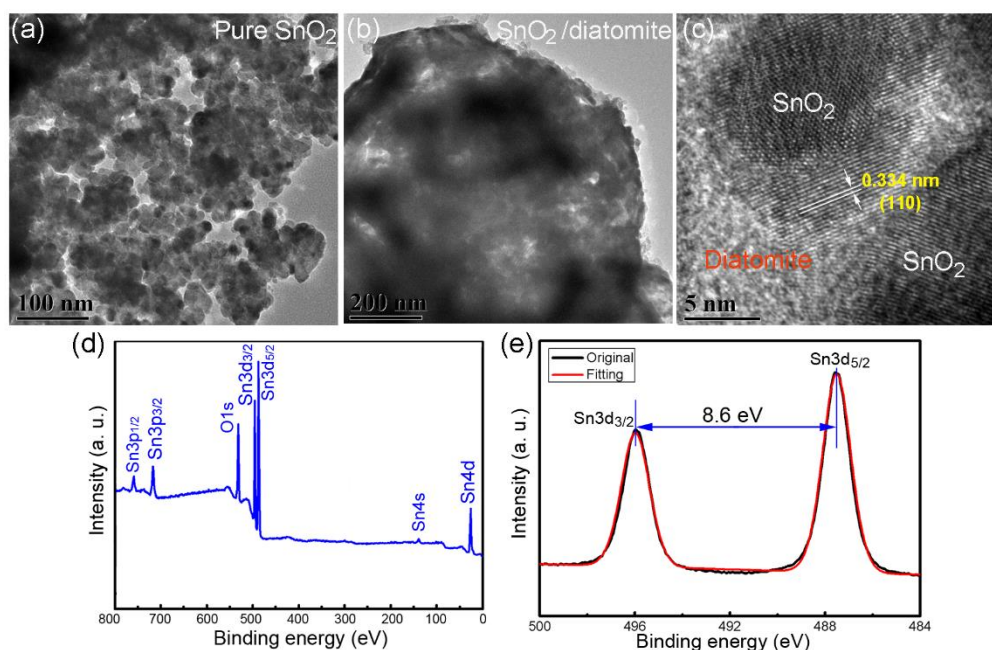


Figure 3. The microstructure of (a) pure SnO_2 and (b,c) SnO_2 /diatomite-SD2 by TEM, and the XPS spectrum of pure SnO_2 (d,e).

The specific surface area of diatomite and SnO_2 /diatomite composites were tested by N_2 adsorption-desorption isotherm (BET) in Figure 4, and corresponding data were listed in Table 1. The specific surface area of modified diatomite was $13.72 \text{ m}^2 \cdot \text{g}^{-1}$. After loading with SnO_2 nanoparticles, the SD2 sample exhibited the maximum specific surface area of $23.53 \text{ m}^2 \cdot \text{g}^{-1}$, which was attributed to

the uniform distribution of SnO₂ nanoparticles. On the contrary, the specific surface area of SD1 and SD3 samples was 17.15 and 14.95 m²·g⁻¹ respectively, and the SD4 sample had the minimum specific surface area of 11.56 m²·g⁻¹, even less than that of modified diatomite. The result further confirms that the much more SnO₂ aggregates loading on the diatomite only increase the sample weight, which reduces the specific surface area of sample and brings a negative effect on the photocatalytic activity, which will be discussed later.

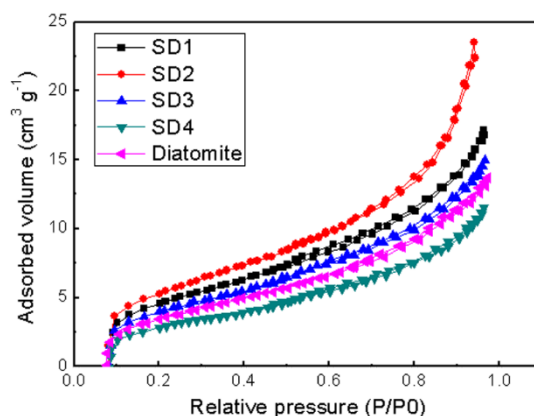


Figure 4. N₂ adsorption-desorption isotherm of diatomite and different SnO₂/diatomite composites.

2.2. Photocatalytic Performance and Photodegradation Mechanism

The photodegradation performance of pure SnO₂ and different SnO₂/diatomite composites in Rh B solution is given in Figure 5. Figure 5a shows the change of adsorption peaks of SD2 sample in Rh B dye for different time. The peak at 546 nm just reflects the typical feature of Rh B. The decrease of peak intensity just shows the concentration change of dye. According to the relationship between the absorption peak intensity and the dye concentration, taking C_t/C_0 as the ordinate and time as the horizontal ordinate, Figure 5b reflects the degradation efficiency curves of different photocatalysts. In the first 3 h, the degradation curves have no obvious change in dark condition, which is mainly due to the physical adsorption of dye on porous diatomite in the dark adsorption process. Under the irradiation of UV-light, pure dye (void) and diatomite have no obvious change, which indicates that the Rh B solution cannot be degraded by diatomite under light irradiation. While pure SnO₂ and four SnO₂/diatomite composites exhibit different photodegradation efficiencies. It can be observed that the photodegradation efficiency order is SnO₂ > SD2 > SD1 > SD3 > SD4. Pure SnO₂ has the best photocatalytic activity for the absence of inert diatomite template. However, when the irradiation time is more than 60 min, SD2 sample almost has the same photocatalytic activity with pure SnO₂ and degrades Rh B dye by 96.8%. The main reason is attributed to the largest specific surface area, and the uniform distribution of SnO₂ nanoparticles on the surface of diatomite. On the contrary, SD4 sample with the largest content of SnO₂ exhibits the worst photodegradation activity, which is due to the smallest specific surface area and the SnO₂ aggregates on diatomite. In addition, we also chose MB solution as a simulated pollutant and observed the degradation efficiency of pure SnO₂ and different SnO₂/diatomite composites. As shown in Figure 5c, the peak at 654 nm denotes the typical feature of MB, and the fading of peak intensity reflects the degradation of MB dye. Figure 5d shows the photocatalytic activity of different samples. Under the UV-light irradiation, the MB solution cannot be degraded by diatomite alone. The photocatalytic activity order of samples is SnO₂ > SD2 > SD1 > SD3 > SD4. The photocatalytic activity for degrading MB solution is completely consistent with Rh B. Under the irradiation of 60 min, SD2 sample has the fastest degradation rate of 96.97%, which is close to that of pure SnO₂. The result indicates that SD2 sample has a better photocatalytic activity in the degradation of MB dye.

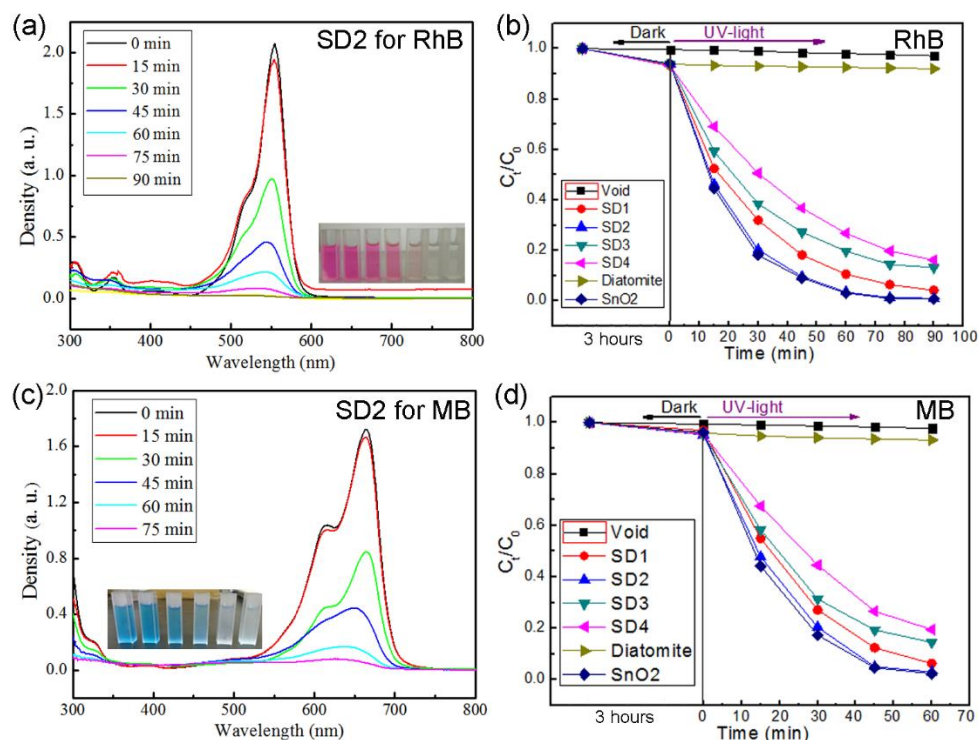


Figure 5. (a) UV-visible adsorption spectra of SD2 sample in Rh B solution under different irradiation time; (b) Photodegradation curves of different samples in Rh B solution; (c) UV-visible adsorption spectra of SD2 sample in MB solution under different irradiation time; (d) Photodegradation curves of different samples in MB solution.

We also simulate the photodegradation behavior of Rh B and MB dye solution according to the first-order reaction kinetic equation of $\ln(C_0/C_t) = k \cdot t$ [18], in which, k is the first-order reaction rate constant; C_0 is the initial concentration of dye; C_t is the dye concentration under different irradiation time, and t is the irradiation time. Figure 6a,b shows the first-order kinetic fitting curves of photodegradation behavior of Rh B and MB dye, respectively. Corresponding k values and curve fitting degrees (R^2) are listed in Table 2. The value of first-order reaction rate constant (k) denotes the slope of the fitting straight line, which reflects the photocatalytic efficiency or degradation rate. While the value of curve fitting degrees (R^2) reflects the coincidence degree of first order reaction kinetics equation. When degrading Rh B dye, the constant k of four samples is 0.035, 0.054, 0.023 and 0.021 min^{-1} , respectively. SD2 sample has the largest k value of 0.054 min^{-1} , indicating the best photocatalytic activity. Moreover, the R^2 value is 0.989, which confirms that the degradation process of Rh B is in good agreement with the first-order reaction kinetic equation. Meanwhile, when these samples are used to degrade MB dye, the constant k is 0.047, 0.061, 0.033 and 0.028 min^{-1} respectively. SD2 sample also exhibits the best photocatalytic activity with the largest k value of 0.061 min^{-1} . The value of R^2 is 0.981, which is in accordance with the first-order reaction kinetic equation. The k value in degradation of MB (0.061) is slightly higher than that of degrading Rh B (0.054), which reflects that the SD2 sample degrades the MB dye much easier.

Table 2. Corresponding first-order reaction kinetic fitting parameters of samples in Rh B and MB.

Sample/Dye	SD1/RhB	SD2/RhB	SD3/RhB	SD4/RhB	SD1/MB	SD2/MB	SD3/MB	SD4/MB
k/min^{-1}	0.035	0.054	0.023	0.021	0.047	0.061	0.033	0.028
R^2	0.997	0.989	0.971	0.996	0.998	0.981	0.985	0.996

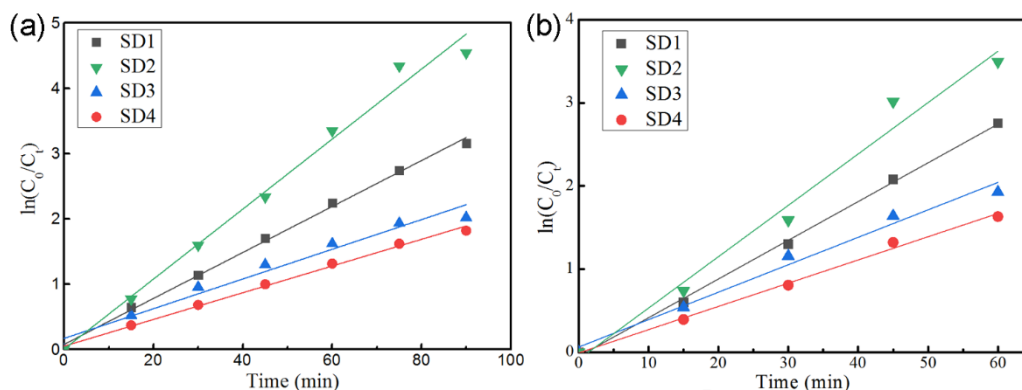


Figure 6. The first-order reaction kinetic fitting curves of (a) Rh B solution and (b) MB solution.

To sum up, the photodegradation behavior of organic dyes mainly depends on the specific surface area and the dispersion state of SnO₂ nanoparticles. Among these samples, SnO₂/diatomite composite (SD2) has the maximum specific surface area of 23.53 m²·g⁻¹, and numerous SnO₂ nanoparticles are dispersed on the surface of porous diatomite template uniformly. Therefore, SD2 sample has the best photocatalytic activity, which is close to the pure SnO₂. Under the irradiation of 60 min, the degradation rate of Rh B and MB dye is 96.8% and 96.97%, respectively.

In order to confirm the absorption feature of SnO₂ and SnO₂/diatomite composite, we observed their UV-vis absorption spectra in Figure 7. Compared to the absorption spectrum of pure SnO₂, the SnO₂/diatomite has a weak light absorption intensity and a narrow light absorption range. The reason can be attributed to the poor light absorption performance of diatomite. Therefore, the porous diatomite template weakens the light absorption of pure SnO₂ in a certain extent. However, from the perspective of overcoming the aggregation of SnO₂ nanoparticles and low-cost of diatomite, the composite of SnO₂/diatomite has a practical application value.

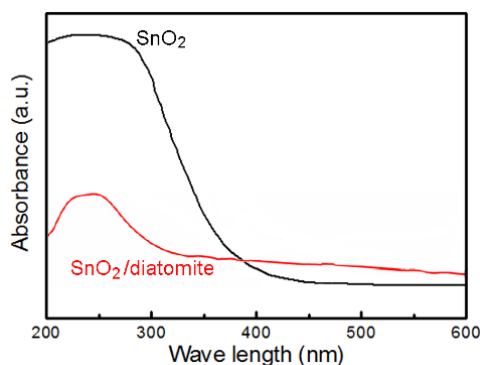
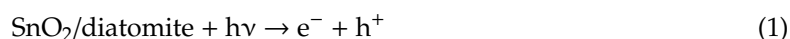


Figure 7. UV-vis absorption spectra of SnO₂ and SnO₂/diatomite.

The photocatalytic mechanism of SnO₂/diatomite composite is put forward in Figure 8. The monodispersed SnO₂ nanoparticles loading on porous diatomite is prepared by adjusting the mass of SnCl₄·5H₂O precursor. When the SnO₂/diatomite powders dispersed in the dye solution, the dye molecules physically adsorb to the disc-shaped surface and pores of the diatomite [19–21], and dye molecules contact with SnO₂ nanoparticles closely. Under the irradiation of UV-light, the electrons in SnO₂ nanoparticles are excited from the valence band to the conduction band, which generates photogenerated electrons and holes. The electrons and holes then diffuse to the surface of SnO₂ catalyst. The redox reaction occurs between electrons/holes and oxygen in water adsorbed on the sample surface, producing some free radicals (•OH and •O₂⁻) with strong oxidation [22,23], just as the following reaction equations [8]:



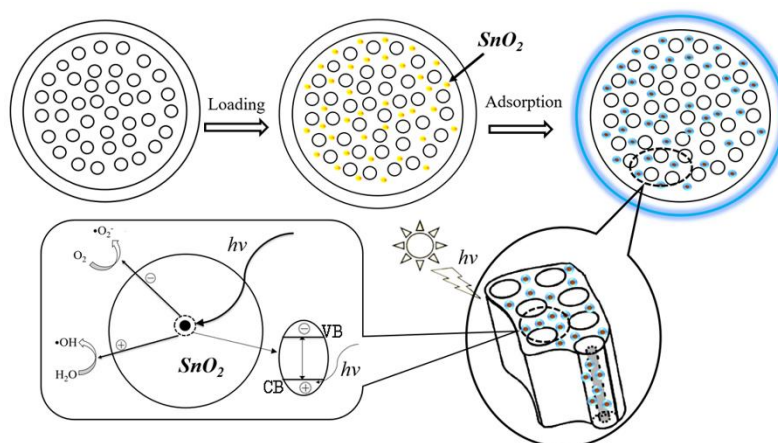
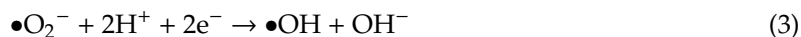


Figure 8. Photocatalytic mechanism of SnO₂/diatomite composite in degradation of organic dyes.

These free radicals oxidize the Rh B and MB molecules into CO₂ and H₂O, and degrade the organic dyes effectively without any secondary pollution. Among the existing diatomite-based composites, the TiO₂/diatomite prepared by hydrolysis-deposition method had a Rh B decoloration rate of 100% within 30 min [24]. Granulated N-doped TiO₂/diatomite exhibited a Rh B degradation rate of 84.8% within 3 h [16]. While pure SnO₂ nanoparticles prepared by precipitation method achieved the degradation of MB (79%) under the irradiation time of 180 min [22]. Hierarchical SnO₂ ultrathin nanosheets degraded 93% of MB within 150 min [25]. Iridium (Ir) nanoparticles decorated SnO₂ nanorods decomposed more than 97% of MB under 60 min irradiation [26]. In this work, the monodispersed SnO₂ decorated diatomite composite achieved the fast degradation of Rh B (96.8%) and MB (96.97%) within 60 min. Through a comparison, the composite photocatalyst present an excellent photodegradation activity. Considering the low cost of diatomite (~3.4 USD per 1000 g), the high fraction of diatomite (above 90%), and easy preparation of SnO₂ nanoparticles, the SnO₂/diatomite composite has a good application prospect in the photodegradation of organic dyes.

3. Materials and Methods

3.1. Materials

SnCl₄·5H₂O, thioacetamide (TAA), absolute ethanol and isopropanol were analytical purity, provided by Sinopharm Chemical Reagent Co. Ltd. (Shanghai, China). Diatomite (industrial grade) was purchased from Qingdao Shengtai Industry Co. Ltd. (Qingdao, China). Organic dye of Rhodamine B (Rh B, analytical purity) and methylene blue (MB, analytical purity) were provided by Nanjing Chemical Reagent Co. Ltd. (Nanjing, China).

3.2. Preparation of Modified Diatomite and SnO₂/Diatomite Composites

In order to obtain a perfect porous structure of diatomite, 10 g diatomite was added into 100 mL dilute hydrochloric acid (1 mol L⁻¹). The suspension was put into a water bath at 80 °C and stirred for 2 h. Then, the solution was cooled to room temperature, and the acidified diatomite was filtered and rinsed to neutral by using abundant distilled water. After drying at 60 °C for 12 h, the acidified diatomite was sintered at 450 °C for 1 h to obtain modified diatomite. 1 g modified diatomite was added into 40 mL isopropanol, and the suspension was stirred continuously. Then, 106 mg

$\text{SnCl}_4 \cdot 5\text{H}_2\text{O}$ and 64 mg TAA were added into the suspension and stirred for 10 min. The suspension was transferred to a 100 mL PTFE-lined stainless-steel autoclave. The solvothermal reaction was carried out at 180 °C for 24 h. The precipitate was filtered and rinsed by ethanol and distilled water respectively to remove the impurities and ions, and SnS_2 /diatomite was obtained after drying at 60 °C for 12 h [15]. The SnS_2 /diatomite was sintered at 500 °C for 2 h in a muffle furnace to obtain SnO_2 /diatomite composite. Following this method, other three SnO_2 /diatomite composites were prepared by adjusting the mass of $\text{SnCl}_4 \cdot 5\text{H}_2\text{O}$ and TAA precursor as 212 and 128 mg, 338 and 192 mg, 424 and 256 mg. According to the addition of precursors, four samples were denoted as SD1, SD2, SD3, and SD4, respectively. In addition, based on the weight difference between modified diatomite and resultant SnO_2 /diatomite, we calculated the fractions of SnO_2 in composite as 4.9%, 7.6%, 11.7% and 16.5%, respectively. The specific recipe of sample is given in Table 1. In order to make a comparison, pure SnO_2 powder was synthesized under the same procedures with no diatomite template.

3.3. Characterization

X-ray diffraction spectrum (XRD) was tested on X-Ray Spectrometer of X-7000 (SHIMADZU, Beijing, China) with a radiation source of $\text{Cu K}\alpha$. Specific surface area was obtained by using Brunauer-Emmett-Teller (BET) method in Micromeritics Instrument (ASAP 2020, Shanghai, China). Scanning electron microscopy (SEM) and transmission electron microscopy (TEM) was conducted on JSM-7500F (JEOL, Beijing, China) and JEM-2010 (JEOL, Beijing, China) separately. X-ray photoelectron spectroscopy (XPS, Thermo Scientific, Shanghai, China) was used with a K-Alpha⁺ photoelectron spectrometer. The photodegradation performance of samples were tested on ultraviolet-visible spectrophotometer (TU-1810, Beijing Persee Tongyong Instrument Co. Ltd., Beijing, China).

3.4. Photocatalytic Measurement

Rh B and MB served as simulated pollutants, and the concentration of two solutions were controlled as 10 mg L⁻¹. The photocatalyst concentration in dye solution was fixed as 500 mg L⁻¹. The experiment detail was given: 50 mg photocatalyst was added into 100 mL pollutant solution, and placed it in a dark chamber for 3 h to uniformly adsorb the dye molecules. Then, the suspension was transferred into a photochemistry reactor irradiated by a mercury lamp (500 W). Under the continuously stirring and irradiation of ultraviolet light, the dye solution (about 5 mL) was taken out from the photodegradation solution in a fixed time interval [8]. The supernatant was obtained by centrifuging the extracted dye solution and measured by using an ultraviolet-visible (UV-vis) spectrophotometer to check the change of dye featured peaks. The photodegradation rate of dye solution was obtained by the concentration change of dye under a fixed illumination time, which reflected the photocatalytic efficiency of photocatalysts. In this work, five photocatalysts were involved, including four SnO_2 /diatomite composites (SD1, SD2, SD3 and SD4) and pure SnO_2 .

4. Conclusions

In summary, SnO_2 /diatomite composite was synthesized by solvothermal reaction and sintering method. In the synthesis process, the weight of reactants was adjusted to effectively overcome the agglomeration of SnO_2 nanoparticles. When the mass of $\text{SnCl}_4 \cdot 5\text{H}_2\text{O}$ and TAA was 212 and 128 mg, monodispersed SnO_2 nanoparticles were uniformly generated on porous diatomite template with a particle size of about 15 nm (SD2). The SD2 composite has the maximum specific surface area of 23.53 m²·g⁻¹. When served as a photocatalyst to degrade Rh B, and MB dye, it presented a superior degradation activity close to pure SnO_2 , and achieved a fast degradation of 96.8% Rh B and 96.97% MB in 60 min. The degradation process of Rh B and MB was in accordance with the first-order kinetic equation. The superior photocatalytic performance of SnO_2 /diatomite composite is attributed to the physical adsorption of dye molecules on the surface and pores of diatomite, and the highly efficient photocatalytic activity of monodispersed SnO_2 nanoparticles. In addition, the SnO_2 /diatomite

composite has the advantages of a low cost and easy preparation, and thus presents good application prospects in the field of photocatalysis.

Author Contributions: Conceptualization, H.J. and X.H.; methodology, H.J. and R.W.; Writing, H.J.; validation, D.W. and S.Y.

Funding: This research was funded by National Natural Science Foundation of China (51403094 and 51774175), and Program of Liaoning Education Department of China (No. LJ2017FBL002).

Conflicts of Interest: The authors declare no conflict of interest.

References

1. Lin, L.; Huang, J.; Li, X.; Abass, M.A.; Zhang, S. Effective surface disorder engineering of metal oxide nanocrystals for improved photocatalysis. *Appl. Catal. B Environ.* **2017**, *203*, 615–624. [[CrossRef](#)]
2. Xu, K.; Wu, J.; Tan, C.F.; Ho, G.W.; Wei, A.; Hong, M. Ag-CuO-ZnO metal-semiconductor multiconcentric nanotubes for achieving superior and perdurable photodegradation. *Nanoscale* **2017**, *9*, 1154–11583. [[CrossRef](#)] [[PubMed](#)]
3. Manjula, P.; Boppella, R.; Manorama, S.V. A facile and green approach for the controlled synthesis of porous SnO₂ nanospheres: Application as an efficient photocatalyst and an excellent gas sensing material. *ACS Appl. Mater. Inter.* **2012**, *4*, 6252–6260. [[CrossRef](#)] [[PubMed](#)]
4. Sinha, A.K.; Pradhan, M.; Sarkar, S.; Pal, T. Large-scale solid-State synthesis of Sn-SnO₂ nanoparticles from layered SnO by sunlight: A material for dye degradation in water by photocatalytic reaction. *Environ. Sci. Technol.* **2013**, *47*, 2339–2345. [[CrossRef](#)] [[PubMed](#)]
5. Li, P.; Lan, Y.; Zhang, Q.; Zhao, Z.; Pullerits, T.; Zheng, K.; Zhou, Y. Iodinated SnO₂ quantum dots: A facile and efficient approach to increase solar absorption for visible-light photocatalysis. *J. Phys. Chem. C* **2016**, *120*, 9253–9262. [[CrossRef](#)]
6. Chen, X.; Chu, D.; Wang, L.; Hu, W.; Yang, H.; Sun, J.; Zhu, S.; Wang, G.; Tao, J.; Zhang, S. One-step synthesis of novel hierarchical flower-like SnO₂ nanostructures with enhanced photocatalytic activity. *J. Alloy. Compd.* **2017**, *729*, 710–715. [[CrossRef](#)]
7. Zhao, Q.; Gao, Y.; Bai, X.; Wu, C.; Xie, Y. Facile synthesis of SnO₂ hollow nanospheres and applications in gas sensors and electrocatalysts. *Eur. J. Inorg. Chem.* **2006**, *8*, 1643–1648. [[CrossRef](#)]
8. Hong, X.; Wang, R.; Li, S.; Fu, J.; Chen, L.; Wang, X. Hydrophilic macroporous SnO₂/rGO composite prepared by melamine template for high efficient photocatalyst. *J. Alloy. Compd.* **2019**. [[CrossRef](#)]
9. Chen, Y.; Sun, F.; Huang, Z.; Chen, H.; Zhuang, Z.; Pan, Z.; Long, J.; Gu, F. Photochemical fabrication of SnO₂ dense layers on reduced graphene oxide sheets for application in photocatalytic degradation of p-Nitrophenol. *Appl. Catal. B Environ.* **2017**, *215*, 8–17. [[CrossRef](#)]
10. Wei, J.; Xue, S.L.; Xie, P.; Zou, R. Synthesis and photocatalytic properties of different SnO₂ microspheres on graphene oxide sheets. *Appl. Surf. Sci.* **2016**, *376*, 172–179. [[CrossRef](#)]
11. Wang, B.; Zhang, G.; Leng, X.; Sun, Z.; Zheng, S. Characterization and improved solar light activity of vanadium doped TiO₂/diatomite hybrid catalysts. *J. Hazard. Mater.* **2015**, *285*, 212–220. [[CrossRef](#)] [[PubMed](#)]
12. Zhang, J.; Wang, X.; Wang, J.; Wang, J.; Ji, Z. Effect of sulfate ions on the crystallization and photocatalytic activity of TiO₂/diatomite composite photocatalyst. *Chem. Phys. Lett.* **2016**, *643*, 53–60. [[CrossRef](#)]
13. Zhong, X.; Shen, Y.; Zhao, S.; Chen, X.; Han, C.; Wei, D.; Fang, P.; Meng, D. SO₂ sensing properties of SnO₂ nanowires grown on a novel diatomite-based porous substrate. *Ceram. Int.* **2019**, *45*, 2556–2565. [[CrossRef](#)]
14. Zhen, Y.; Zhang, J.; Wang, W.; Li, Y.; Gao, X.; Xue, H.; Liu, X.; Jia, Z.; Xue, Q.; Zhang, J.; et al. Embedded SnO₂/diatomaceous earth composites for fast humidity sensing and controlling properties. *Sens. Actuat. B Chem.* **2020**, *303*, 127137. [[CrossRef](#)]
15. Hong, X.; Li, S.; Wang, R.; Fu, J. Hierarchical SnO₂ nanoclusters wrapped functionalized carbonized cotton cloth for symmetrical supercapacitor. *J. Alloy. Compd.* **2019**, *775*, 15–21. [[CrossRef](#)]
16. Chen, Y.; Liu, K. Preparation of granulated N-doped TiO₂/diatomite composite and its applications of visible light degradation and disinfection. *Powder Technol.* **2016**, *303*, 176–191. [[CrossRef](#)]
17. Jia, B.; Jia, W.; Qu, F.; Wu, X. General strategy for self assembly of mesoporous SnO₂ nanospheres and their applications in water purification. *RSC Adv.* **2013**, *3*, 12140–12148. [[CrossRef](#)]

18. Vishnuganth, M.A.; Remya, N.; Kumar, M.; Selvaraju, N. Photocatalytic degradation of carbofuran by TiO₂-coated activated carbon: Model for kinetic, electrical energy per order and economic analysis. *J. Environ. Manag.* **2016**, *181*, 201–207. [[CrossRef](#)]
19. Chen, Y.; Liu, K. Preparation and characterization of nitrogen-doped TiO₂/diatomite integrated photocatalytic pellet for the adsorption-degradation of tetracycline hydrochloride using visible light. *Chem. Eng. J.* **2016**, *302*, 682–696. [[CrossRef](#)]
20. Zhang, G.; Sun, Z.; Duan, Y.; Ma, R.; Zheng, S. Synthesis of nano-TiO₂/diatomite composite and its photocatalytic degradation of gaseous formaldehyde. *Appl. Surf. Sci.* **2017**, *412*, 105–112. [[CrossRef](#)]
21. Chen, Y.; Wu, Q.; Zhou, C.; Jin, Q. Enhanced photocatalytic activity of La and N co-doped TiO₂/diatomite composite. *Powder Technol.* **2017**, *322*, 296–300. [[CrossRef](#)]
22. Kim, S.P.; Choi, M.Y.; Choi, H.C. Photocatalytic activity of SnO₂ nanoparticles in methylene blue degradation. *Mater. Res. Bull.* **2016**, *74*, 85–89. [[CrossRef](#)]
23. Chen, H.; Pu, X.; Gu, M.; Zhu, L.; Chen, L. Tailored synthesis of SnO₂@graphene nanocomposites with enhanced photocatalytic response. *Ceram. Int.* **2016**, *42*, 17717–17722. [[CrossRef](#)]
24. Chen, H.; Pu, X.; Gu, M.; Zhu, L.; Chen, L. The influence of carriers on the structure and photocatalytic activity of TiO₂/diatomite composite photocatalysts. *Adv. Powder Technol.* **2015**, *26*, 595–601.
25. Huang, R.; Huang, S.; Chen, D.; Zhang, Q.; Le, T.; Wang, Q.; Hu, Z.; Chen, Z.; Jiang, Y.; Zhao, B. Insight into efficient pollutant degradation from paramorphic SnO₂ hierarchical superstructures. *J. Alloy. Compd.* **2019**, *776*, 287–296. [[CrossRef](#)]
26. Dhanalakshmi, M.; Saravanakumar, K.; Prabavathi, S.L.; Abinaya, M.; Muthuraj, V. Fabrication of novel surface plasmon resonance induced visible light driven iridium decorated SnO₂ nanorods for degradation of organic contaminants. *J. Alloy. Compd.* **2018**, *763*, 512–524. [[CrossRef](#)]



© 2019 by the authors. Licensee MDPI, Basel, Switzerland. This article is an open access article distributed under the terms and conditions of the Creative Commons Attribution (CC BY) license (<http://creativecommons.org/licenses/by/4.0/>).